Driving of Strong Nightside Reconnection and Geomagnetic Activity by Polar Cap Flows: Application to CME Shocks and Possibly Other Situations

L. R. Lyons[1], B. Gallardo-Lacourt[1,6], Y. Zou[2], Y. Nishimura[1,3], P Anderson[4], V. Angelopoulos[5], E. F. Donovan[6], J. M. Ruohoniemi[7], E. Mitchell[8], L. J. Paxton[8], and N. Nishitani[9]

[1]Department of Atmospheric and Oceanic Sciences, University of California, Los Angeles, CA 90095-1565, USA (larry@atmos.ucla.edu)

[2]Center for Space Physics and Department of Astronomy, Boston University, Boston MA 02215

[3]Center for Space Physics and Department of Electrical and Computer Engineering, Boston University, Boston, MA 02215

[4]Department of Physics, The University of Texas at Dallas, 800 W. Campbell Road Richardson, Texas 75080-3021

[5]Department of Earth, Planetary, and Space Sciences, University of California, Los Angeles, CA 90095-1567, USA.

[6]Department of Physics and Astronomy, University of Calgary, 2500 University Drive, Calgary, Alberta, Canada T2N 1N4

[7]Bradley Department of Electrical and Computer Engineering, Virginia Tech, Blacksburg, VA 24061, USA

[8]Johns Hopkins University Applied Physics Laboratory, Laurel, MD, 20723, USA.

[9]Institute for Space-Earth Environmental Research, Nagoya University, Nagoya, Aichi 464-8601, Japan

Submitted to

Journal of Atmospheric and Solar-Terrestrial Physics, Special Issue:
"Dynamics of the Sun-Earth System: Recent Observations and Predictions"

April 2017

Corresponding author: L. R. Lyons: larry@atmos.ucla.edu

Abstract

Previous studies have shown that dynamic pressure impacts (e.g., shocks initiating CME storms) with southward IMF promptly lead to strong auroral nightside activity and concurrent poleward expansion (indicating strong nightside reconnection), and strong enhancements in convection and currents. Here we use a combination of ground-based ASI and radar observations to further describe this response, to address what is driving the strong activity, and to suggest similar driving in other situations. Consistent with some previous studies, we find that shock driven auroral activity and poleward expansion resembles a substorm, but starts from an already broad MLT sector without much subsequent azimuthal expansion and without classical brightening of the equatorward-most arc. We furthermore find a large enhancement of meso-scale ionospheric polar cap flows heading towards the nightside separatrix immediately after shock impact. Recent studies have shown that such enhanced flows often cross the separatrix leading to plasma sheet flow bursts, poleward boundary intensifications (PBIs), streamers, and poleward motion of the polar cap boundary from reconnection. Thus these flow enhancements, which must extent outward along field lines from the ionosphere, are an attractive candidate as the driver for the almost immediate strong auroral, current, and reconnection activity resulting from shock impact. We also discuss and present some evidence that this phenomenon may be more general, leading to similar oval responses without a shock impact, including during and following the expansion phase some substorms. These suggestions could lead to some possibly fundamental questions, such as when do polar cap convection enhancements lead to a substorm growth phase versus leading directly to strong polar expansion of, and strong activity along, the auroral oval field line region?

Keywords: Magnetic storms; aurora; convection; polar cap; substorm; reconnection

1. Introduction

Abrupt enhancements of solar wind dynamic pressure (P_{dyn}), such as the shocks that initiate coronal mass ejection (CME) storms, cause dramatic effects when they occur under southward interplanetary magnetic field (IMF) conditions. They drive nearly immediately strong auroral activity, poleward expansion of the auroral oval that can reach as much as 10^o in latitude, and strong enhancement in global convection, ionospheric currents, and Region 1 and Region 2 field-aligned currents (Boudouridis, 2003; Lyons et al., 2016; Zesta et al., 2000). The rapid poleward expansion of the nightside auroral oval implies strong nightside reconnection in the presence of a nearly simultaneous increase in the strength of convection.

The nightside auroral activity resembles a substorm, but initiates over a substantially broader range of MLT without much subsequent azimuthal expansion as poleward expansion occurs over a broad longitudinal range (Chua et al., 2001; Lyons et al., 2000; Zesta et al., 2000). These and other features, such as the lack of brightening of an equatorward arc, have lead to the suggestion that the disturbance is different from substorms (Liou et al., 2003; Yue et al., 2013). However, other studies have indicated that the disturbance may be a substorm (Kokubun et al., 1977; Lyons, 2005; Zhou and Tsurutani, 2001), and dipolarizations as occur during substorms are seen at geosynchronous orbit in response to solar wind dynamic pressure impacts on the magnetosphere (Lee et al., 2005; Lee and Lyons, 2004).

In this paper, we describe the dramatic nightside response using modern ground-based all-sky imager (ASI), radar, and low-altitude spacecraft observational capabilities, and we address what is driving the strong auroral, current, and reconnection activity. We take particular advantage of the 17 March 2013 storm, a CME-driven event initiated by a shock that impacted the magnetosphere at 06 UT (Baker et al., 2014). There has been much interest in ring current particle injections (e.g., *Gkioulidou et al., 2014)* and radiation belt electrons (Hudson et al., 2015; Li et al., 2014, 2015) for this event. Of importance for the current study is the excellent radar and auroral observation coverage at times just before and just after the shock impact (Lyons et al., 2016; hereafter referred to as Paper 1), allowing for excellent evaluation of the effects of the shock. Consistent with some previous studies, we find that the onset of the shock-driven activity appears to be very different from the onset of a substorm. However, we find that the activity following shock impact appears to be driven by enhancements of meso-scale flows along polar-cap field lines, and this has important similarities to what has been suggested to drive prolonged activity during the expansion phase of some substorms. This, and additional evidence we present here, suggest that the driving of activity we show here may apply more generally than just to the impact of P_{dyn} enhancements.

2. Observations

Observations for the magnetic storm on 17 March 2013 in Paper 1 show that the shock impact with concurrent southward IMF immediately drove dramatic poleward expansion of the poleward boundary of the auroral oval (implying strong nightside reconnection), strong auroral activity, and strong penetrating mid-latitude convection and ionospheric and field-aligned currents. Figure 1 shows, from top to bottom, the WIND solar wind dynamic pressure P_{dyn}, the OMNI interplanetary magnetic field (IMF) as propagated to the dayside magnetopause, the SuperMAG (Gjerloev, 2012) ground magnetometer upper U and lower L auroral magnetic index, and the SuperMAG ring current index for all MLT and within the dusk, noon, dawn, and midnight sectors. The SuperMAG indices are based on the traditional AU, AL, and SYMH indices, but with many more stations. The OMNI IMF data is shown further shifted by ~10 minutes so that the shock impact time agrees with the 0600 UT impact time seen by the dayside ground magnetometers. The WIND P_{dyn} is shown because of data gaps in the OMNI P_{dyn} around the time of the shock and is further shifted by ~30 min relative to the IMF data to agree with the time of shock impact.

The U and L indices reflect immediate and large increases in ionospheric current that were driven when the shock impacted the magnetosphere, as indicated by the large increase in P_{dyn}. The lower panels show the strong increases in Region 1 and Region 2 currents that were seen from AMPERE magnetic perturbations observed along Iridium satellite trajectories during the 10 min interval immediately before, and the second 10 min interval after, the shock impact. Red and blue shadings give upward and downward FACs, respectively, obtained from the curl of fits to the magnetic perturbations (Waters et al., 2001).

Figure 2 shows mergers of auroral images over Canada from the array of THEMIS ASIs (Mende et al., 2008) overlaid with line-of-sight (LOS) flow velocities from the Super Dual Auroral Radar Network (SuperDARN) radars from the period a few min before to 18 min after the P_{dyn} impact. The ASI images are displayed so as to emphasize the radar echoes within the polar cap from the pair of PolarDARN radars (Koustov et al., 2009) at Inuvik to the west and Rankin Inlet to the east. Observations from the lower latitude SuperDARN radars have been emphasized in Paper 1. The top three panels of Figure 2 show a narrow band of moderately active aurora that lay along the poleward boundary of the evening-to-midnight auroral oval prior to the shock impact. This activity, and the lower than average location of the auroral poleward boundary (magnetic latitude $\Lambda \sim 68^{o}$ -70^{o}), likely resulted from the pre-storm southward IMF of a few nT. The dramatic enhancement in activity and poleward expansion of the auroral oval that initiated almost immediately after the shock impact can be seen over several hours of MLT in the next four panels (0602 to 0611 UT) of Figure 2, as well as in movie S1 in paper 1. This includes a rapid, large poleward expansion of the auroral oval over a broad MLT range.

The enhancement and poleward expansion of the aurora also shows vividly in the auroral observations from the Special Sensor Ultraviolet Spectrographic Imager (SSUSI) (http://ssusi.jhuapl.edu/) onboard polar-orbiting Defense Meteorological Satellite

Program (DMSP) spacecraft in Figure 3. SSUSI measures FUV emissions in five spectral bands simultaneously (Paxton et al., 2017). Algorithms have been applied to properly remove the dayglow, and the LBH emission intensities shown in Figure 3 reflect precipitating auroral electron energy flux (Paxton et al., 1992, 1998, 1999).

The auroral images in Figure 3 are essentially keograms made along the trajectory of a spacecraft from horizon to horizon imager scans in the direction normal to the trajectory. The DMSP spacecraft had extremely fortuitous crossings of the nightside auroral oval in the southern hemisphere, F17 crossing just 12 to 4 min before the 0600 UT shock impact, and F18 and F16 crossings from 1 to 14 min after the impact. Strong auroral enhancement and poleward expansion can be seen as the F18 and F16 spacecraft passed the dawnside oval at ~0602 to 0604, just 2 to 4 min after shock impact, and the F16 observations show that the oval expanded poleward by ~5^{o} in latitude by ~0606-0607 UT. The poleward expansion can also be seen in the precipitating electron energy fluxes measured by DMSP and plotted along the spacecraft trajectory (the full precipitating particle energy spectra from the F16 and F17 crossings are shown in Figure 3 of Paper 1).

As seen from the SuperDARN observations in Figure 2, LOS velocities were moderately strong within the nightside polar cap during the period preceding the shock impact. They had an anti-sunward LOS component, and show considerable meso-scale structure with longitudinal scales of ~0.5 to 1 hr in MLT. Immediately following the impact, the anti-sunward LOS ionospheric flows seen by the radars and their meso-scale structure enhanced considerably within the polar cap region encircled by the ellipses, and peak values above 600 m/s can be seen directed towards the nightside auroral oval. These flows can be seen down to magnetic latitudes Λ of ~ 77-78^{o}, just a few degrees poleward of the expanded auroral oval. (The few radar echoes at Λ ~ 73-76^{o} are echoes for the E-region, where speeds are substantially reduced from the electric field drift speed). The polar cap flows and auroral activity decreased approximately simultaneously starting at

0614 UT, as the IMF briefly turned northward. A similar enhancement of polar cap flows and their meso-scale structure can be seen in SuperDARN observations in Figure 3 from the southern hemisphere SuperDARN radars. In Figure 3, enhanced polar cap flows seen by SuperDARN near midnight and near 04 MLT appear to impact the poleward boundary of the auroral oval. The inference is supported by the flows measured by the DMSP F17 and F16 spacecraft in the direction normal to the spacecraft trajectory, these flows being shown by the violet bars in Figure 3.

Figure 4 shows the poleward expansion of the oval in the southern hemisphere based on the precipitating electron energy fluxes from both the Polar Operational Environmental Satellites (POES) and the DMSP spacecraft. Though the two post-shock POES passes crossed the nightside auroral oval several minutes after the shock-related activity started to subside, they clearly show that the oval poleward boundary had expanded to $\Lambda \sim 78^{\circ}$, which is $\sim 10^{\circ}$ poleward of where it was prior to the shock impact. Figure 4 also includes the polar cap flows seen by SuperDARN at times during the period of rapid auroral poleward expansion. The enhanced flows can clearly be seen to have extended from the polar cap into the region that became occupied by the expanded oval. As in Figure 3, the flows from the polar cap appear to be directed so as to impact the auroral poleward boundary, though the lack of direct observation of flows impacting the auroral poleward boundary prevents definitive determination of whether this occurred.

Before addressing the possible role of the enhanced polar cap flows in the magnetosphere responses to dynamic pressure impacts and their possible generalization to other activity, we discuss observations from two additional storm events initiated by impacts of CME shock increases in P_{dyn} under southward IMF at times appropriate for ASI viewing over North America. The first storm was a CME storm on 19 February 2014 (Durgonics et al., 2017). Figure 5 shows the OMNI interplanetary magnetic field (IMF) and P_{dyn} as propagated to the dayside magnetopause, the SuperMAG ground magnetometer upper U and lower L auroral magnetic index, and the SuperMAG ring current index for all MLT and within the dusk, noon, dawn, and midnight sectors for this event. The OMNI data have been shifted by ~12 minutes so that the shock impact time agrees with the 0348 UT impact time seen in the ring current indices. As for the 17 March 2013 storm, the U and L indices show immediate and large increases in ionospheric current that where driven as the shock impacted the magnetosphere, as indicated by the large increase in P_{dyn}

Figure 6 shows mergers of auroral images over Canada from the THEMIS ASIs overlaid with line-of-sight (LOS) flow velocities from the SuperDARN radars from the period a few min before to 30 min after the shock impact. Moderately active aurora can be seen prior to the impact in the first two panels, the activity likely associated with the substantially negative IMF B_z during that period. Poleward expansion of the oval by a few degrees in latitude and an enhancement in activity can be seen over several hours of MLT during the 20 min period after the shock impact in the next five panels (0350 to 0410 UT) of Figure 2. It can be seen that the rapid, large poleward expansion of the auroral oval occurred over a broad MLT range. The SuperDARN observations in Figure 6 (encircled by the yellow ellipse) show an enhancement of LOS velocities directed anti-sunward within the nightside polar cap during the period of auroral poleward expansion. As indicated by yellow arrows, the observations at 0350 and 0352 UT show enhanced LOS flows at 20-22 MLT (the midnight meridian is given by the blue line) at Λ's from ~68° to 72°. These flows appear to be enhanced over those prior to shock impact, to impinge upon the nightside auroral poleward boundary, and to extend to within the auroral oval. We note that the numbers of radar echoes in this region prior to the shock impact were limited, preventing definitive determination of whether the flows were enhanced by the shock impact.

Enhancement of anti-sunward polar cap flows also occurred in the southern hemisphere for this storm. This can be seen from the SuperDARN LOS flows in Figure 7, the region of the polar cap echoes being quite near the magnetic pole. The poleward expansion of the auroral oval is seen quite clearly in Figure 7 to have been ~5º in latitude by 0357 UT (9 min after shock impact), based on the precipitating electron energy fluxes from the POES spacecraft that are shown in the lower-right panel.

The third event with southward IMF had an onset at 0826 UT at 5 April 2010 and was studied by Yue et al. (2013) (See their Figure 7-9) and Loto'aniu et al. (2015). (This was the storm that brought down the Galaxy 15 satellite for about 1 year.) Quick and very strong increases in nightside, anti-sunward polar cap flows with meso-scale structure were seen also for this event, as shown by the nightside SuperDARN LOS velocities in Figure 8. For this event, there were THEMIS spacecraft nicely positioned near the northern hemisphere outer boundary of the plasma sheet near midnight at $X_{GSM} = -11.3\ R_E$. These spacecraft saw the initiation of plasma sheet flow bursts just ~2-3 min after the dynamic pressure impact, consistent with the entry of the enhanced meso-scale flow from open polar cap field lines to the plasma sheet. (Note that ionospheric flows impacting the poleward boundary of the auroral oval would be expected to extend outward along field lines into the magnetosphere and impact the outer boundary of the plasma sheet at all X distance along the open-closed field line boundary that lie earthward of the distant magnetic X-line. This is assuming that magnetic field lines are approximately equipotentials and that the poleward boundary of the auroral oval and outer boundary of the plasma sheet both lie along the boundary between open and closed field lines.)

3. Possible role of enhanced polar cap flows

Enhancements in polar cap convection are often viewed as leading to substorm growth phase conditions (Juusola et al., 2011; McPherron, 1970). However, the observations here indicate that, under some conditions, enhancements in polar cap convection can lead to dramatic poleward expansion of, and activity within, the auroral oval, a response that is more like a substorm expansion phase than a substorm growth phase. Based on these observations, we suggest that the enhanced meso-scale polar cap flows heading towards the poleward boundary of the nightside auroral oval may be important for the enhancement of auroral activity and auroral poleward expansion associated with shock impacts. We also address evidence that this phenomenon may be more general than being only a response to abrupt P_{dyn} increases.

A large number of studies have shown that such flows often can cross the auroral poleward boundary, and lead to plasma sheet flow bursts, intensifications along the auroral poleward boundary (PBIs), and auroral streamers (de la Beaujardière et al., 1994; Lyons et al., 2011; Nishimura et al., 2010; Ohtani and Yoshikawa, 2016; Pitkänen et al., 2013; Shi et al., 2012; Zou et al., 2014). This corresponds to externally driven localized reconnection, assuming the auroral poleward boundary is approximately collocated with the open-closed magnetic and flows cross that boundary. Driving of PBIs and streamers by the enhanced polar cap flows may explain the enhancement in auroral activity following the shock impact, which has been found in Paper 1 to consist of streamers. Furthermore, poleward expansion of the auroral poleward boundary has been seen in PBIs that result from incoming meso-scale flows from the polar cap (Zou et al., 2014, 2015). This indicates that poleward expansion of the auroral oval can be a result of the reconnection and PBIs triggered by incoming polar cap flows.

To account for the poleward expansion of the oval that extends over several hours of MLT and brings the auroral poleward boundary poleward by up to several degrees in latitude, enhanced meso-scale flows would have to impact the auroral poleward boundary over the entire longitudinal extend of the auroral poleward expansion and throughout the period of that expansion. Consistent with this, as can be seen from Figures 2, 6, and 8, enhanced flows with meso-scale structuring are seen over ~7-8 hours of MLT within the nightside polar cap and heading towards the auroral poleward boundary. Furthermore, in our cases, the flow initiates as the poleward boundary starts to move poleward. The flows continue as the boundary continues to move poleward, and the flows reduce in magnitude as the poleward motion of the oval ceases and activity decreases within the oval.

A limitation in our observations is that we do not have radar echoes just poleward of the auroral poleward boundary at the time of the shock impact for the 17 March 2013 or 5 April 2010 storms, though we do have a limited number of such echoes for the 19 February 2014 storm. The activity along the auroral poleward boundary just prior to shock impact indicates that enhanced meso-scale flows were impinging on the polar cap boundary prior to the shock impacts. However, it is necessary for such flows to increase with the shock impact as we have seen for the flows a few degrees further poleward in order to account for the nearly simultaneous flow and auroral activity enhancement. While do have the limited direct observation of the enhancement of these flows for the 19 February 2014 storm, as well as direct evidence from the increases observed deeper in the polar cap, we cannot say for certain that, in general, flows adjacent to the polar cap boundary increase at onset. Furthermore, the enhancement in field-aligned currents by the shock compression would be expected to contribute to the shock-associated auroral brightening, though we are not aware of evidence that such currents could contribute to the poleward expansion of the aurora oval following shock impact.

In this paper, we have focused on P_{dyn} increases that initiate CME-driven geomagnetic storms. However, substantially enhanced meso-scale flows occur under other conditions as well, and they may also drive enhanced aurora activity and poleward expansion during these conditions. For example, in one of our earlier substorm studies (Lyons et al., 2011), we noted unexpected observations from a limited number (8) of substorm onsets that had good radar coverage within the polar cap region poleward of substorm expansion phase activity. We found that four of the onsets were followed by prolonged periods of strong ionospheric flow channels directed toward the polar cap boundary from the polar cap. The expansion phases after these onsets had large auroral poleward expansion and prolonged periods of PBI and streamer activity contemporaneous with the enhanced equatorward-directed flow channels. The other four onsets were not followed by such prolonged polar-cap flow channel activity, and the resulting substorm expansions after these onsets were far more limited in duration and in poleward expansion.

The strong poleward expansion and auroral activity that occur during the expansion phase of some substorm, such as the 4 of 8 mentioned above, looks very similar to that following P_{dyn} enhancement impacts. This suggests that strong meso-scale flows (common to both) may be a property of the driver of activity for both situations, suggesting that the post P_{dyn} enhancement impact activity and extended substorm expansion phase activity may be quite similar phenomena. Another variant of this possibility is shown in Figure 9, and appears quite dramatically in the supplemental movie. Figure 9 shows mergers of images from the THEMIS ASIs overlaid with line-of-sight (LOS) flow velocities from the SuperDARN radars for selected times throughout an event that started as a typical substorm onset at ~0803 UT during a storm on 13 October 2010. Onset was identified from a brightening and activity along the equatorward-most arc at $\Lambda \sim 61.5^{o}$. The movie shows the same event at the highest possible time resolution (3 s) of the ASIs (though the time resolution of the radar observations is 1 min). This event was chosen because of the excellent coverage from the Inuvik radar of echoes within the polar cap and within the longitude range of the observed auroral activity.

After onset, the expansion phase activity expanded poleward and azimuthally until, at ~0813 UT, it reached the pre-existing arc that lay along the poleward boundary of the auroral oval (at $\Lambda \sim 66^{o}$, near 21 MLT, and marked by an orange dashed line). The expansion phase aurora subsequently did not protrude further into the pre-existing polar cap region and visible streamers stopped penetrating into the equatorial portion of the oval. Then, at ~0829 UT, the activity enhanced. It began along the auroral poleward boundary, and was followed by poleward expansion to $\Lambda \sim 70^{o}$ and numerous streamers extending to within the equatorward portion of the oval. The radar observations show moderate LOS flows (a few hundred m/s) as the post-onset auroral activity expanded poleward to the pre-existing auroral poleward boundary and became stalled at that boundary. Then, starting at ~0827- 0828 UT, the LOS flow velocities strongly increased to near 1 km/s, and the further auroral activity and poleward expansion commenced at ~0829 UT. Both the flows and activity reduced considerably starting at ~0840 UT. The renewed activity after 0828 UT for this event resembles that from the P_{dyn} enhancements in that the activity started from the polar cap boundary, initiated as the flows directed toward the auroral poleward boundary increased, and decreased as the incoming flows decreased. A difference is that the re-enhancement of auroral activity for this event appears to have occurred ~1-2 min after the first detection of the polar-cap flow increases, indicating that the enhanced flows may have propagated from the dayside. We suggest that the flow enhancement driven by the shock impact likely occurred approximately simultaneously over the entire polar cap, including adjacent to the auroral poleward boundary. Also, the longitudinal extent of the activity was much smaller for this event than for the P_{dyn} enhancement impacts. We suspect that this reflects a smaller longitude range of the enhanced polar cap flows; however, there were not sufficient radar echoes away from the activity region to determine whether or not this was the case.

4. Summary and Conclusions

We have used a combination of ground-based ASI, radar, and low-altitude spacecraft observations to further describe the response of the magnetosphere-ionosphere system to abrupt enhancements of P_{dyn} under southward IMF conditions, such as can occur when CME shocks impact the magnetosphere and lead to magnetic storms. Consistent with previous studies, we find that P_{dyn} enhancements promptly lead to enhanced nightside auroral activity and large auroral poleward expansion, which indicates strong nightside reconnection. The auroral activity and poleward expansion appears to be very similar to what occurs during the expansion phase of substorms, and includes numerous auroral streamers, which indicate plasma sheet flow bursts (as directly seen for the 5 April 2010 event). However, the activity is much broader in MLT, has limited azimuthal expansion, and does not show the classical brightening of the equatorward-most arc that demarcates a substorm onset.

The radar observations within the nightside polar cap have given possible insight into what is driving this shock-driven auroral response, including the associated enhancement in auroral-oval ionospheric and field-aligned currents and in reconnection activity along the auroral poleward boundary. Specifically, we have found a quick and large enhancement of meso-scale polar cap flows heading towards the nightside separatrix after shock impact. Recent studies have shown that such enhanced meso-scale flows often lead to localized, enhanced flows across the nightside separatrix, (i.e, localized reconnection), and that these flows lead to plasma sheet flow bursts, PBIs, and streamers. Furthermore, PBI observations have shown that the polar cap boundary can move poleward associated with the reconnection that results from the impact onto the plasma sheet of enhanced flows from along open, polar cap field lines.

Based on these previous observations, we suggest that the flow enhancements along polar-cap field line that are promptly driven by P_{dyn} enhancement impacts are an attractive candidate for driving the almost immediate strong auroral, current, and reconnection activity resulting from the impact. These flow enhancement after P_{dyn} impact would have to extend to just poleward of the auroral poleward boundary to account for the rapid auroral response of impact. However we are not able to definitively show that this occurred due to the lack of sufficient flow observations adjacent to the aurora boundary at impact. To account for the poleward expansion of the oval that extends over several hours of MLT and brings the auroral poleward boundary poleward by up to several degrees in latitude over a period of several minutes, enhanced meso-scale flows would have to impact the auroral poleward boundary over the entire longitudinal extend of the auroral poleward expansion and such impacts must persist throughout the period of the auroral poleward expansion. The observations presented here are consistent with this scenario, the enhanced flows and their persistence during the period of auroral activity and expansion being seen within regions of polar cap radar echoes. However, we do not have radar echoes over the entire longitude extent of the auroral activity. Additionally, the enhancement in field-aligned currents by the shock impact may be an additional contributor to the shock-associated auroral brightening and current enhancement.

We have also noted that enhanced meso-scale flows along polar-cap field line occur under other conditions, and they may drive enhanced auroral activity and poleward expansion during these conditions. In particular, we have previously found evidence that prolonged periods of auroral activity and auroral poleward expansion during the expansion phase of substorms accompany prolonged periods of strong polar-cap flow channels directed toward the nightside auroral oval boundary. More limited expansion phase activity was seen when such flow channels where absent following substorm onset. In this paper, we presented an example showing variation of this phenomenon. In the example, auroral activity after a substorm onset continued only for the several minutes that it took for the activity to expand poleward to the pre-existing auroral poleward boundary. Then, after a delay of ~15 min, polar cap flows towards the nightside auroral poleward boundary strongly increased to near 1 km/s, and further auroral activity started from along the auroral poleward boundary. This was followed by further auroral poleward expansion and numerous streamers extending to within the equatorward portion of the oval. Both the flows and activity reduced considerably starting at the same time after ~15 min of activity.

It is potentially interesting that we have seen common features of, and possibly common driving of, the activity after P_{dyn} enhancement impacts and following substorm onsets. The common features include auroral activity protruding into the pre-existing polar cap and numerous streamers penetrating towards the equatorial portion of the auroral oval. These common features make activity following P_{dyn} enhancements under southward IMF look very similar to that in post-substorm onset examples. Furthermore, the activity is associated with enhanced meso-scale flows heading towards the nightside separatrix in both sets of cases, and the enhanced flows and activity ceases essentially simultaneously in both sets. It is also interesting that for the P_{dyn} enhancement impact events, and the post-substorm event presented here, activity starts from the auroral polar cap boundary and not from the brightening and breakup of an equatorward auroral arc as in the sequence that initiates a substorm. We thus suggest that enhanced meso-scale flows heading toward the nightside polar cap boundary may be common to the driving of auroral activity that extents into the pre-existing polar cap, and that such events may start from the auroral poleward boundary and may not necessarily be associated with a typical substorm onset.

If further investigation indicates that above suggestion may be true, it would open up some new potentially significant questions. For example, enhancements in polar cap convection are often viewed as leading to substorm growth phase conditions. Under what conditions do such enhancements lead to a substorm growth phase, versus leading directly to strong poleward expansion of, and strong activity within, the region of auroral oval field lines? Another question is what leads to and causes the enhancements in meso-scale polar cap flows. Clearly, enhancements in P_{dyn} do so, but how do they do this? Also, what drives the polar-cap flow enhancements when there is not an enhancement in P_{dyn}? Southward turnings of the IMF are one obvious possibility, but such a turning was not observed for the example presented here.

Acknowledgements

Work at UCLA has been supported by NSF grants AGS-1401822 and AGS-1451911, NASA grant NNX15AI62G 1401822, and the AFOSR Multidisciplinary Research Program of the University Research Initiative (MURI) via subgrant 12602015166:1 from the University of Texas, Arlington. SuperDARN is a collection of radars funded by national scientific funding agencies of Australia, Canada, China, France, Italy, Japan, South Africa, United Kingdom and United States. JMR acknowledges the support of NSF under award AGS-1341918. The SuperDARN data can be obtained from JMR or viewed using the Virginia Tech SuperDARN website at http://vt.superdarn.org/. The DMSP data are maintained by the Air Force Research Laboratory and Applied Physics Laboratory at Johns Hopkins University. We thank the SuperMAG, PI Jesper W. Gjerloev for make the SuperMAG indices available at http://supermag.jhuapl.edu/. We acknowledge NASA contract NAS5-02099 for use of data from the THEMIS Mission, and for the THEMIS ASI observations, we thank S. Mende, the CSA for logistical support in fielding and data retrieval from the GBO stations, and NSF for support of GIMNAST through grant AGS-1004736. We thank Yongliang Zhang for processing the SSUSI auroral observations.

References

Baker, D.N., Jaynes, A.N., Li, X., Henderson, M.G., Kanekal, S.G., Reeves, G.D., Spence, H.E., Claudepierre, S.G., Fennell, J.F., Hudson, M.K., Thorne, R.M., Foster, J.C., Erickson, P.J., Malaspina, D.M., Wygant, J.R., Boyd, A., Kletzing, C.A., Drozdov, A., Shprits, Y.Y., 2014. Gradual diffusion and punctuated phase space density enhancements of highly relativistic electrons: Van Allen Probes observations. Geophys. Res. Lett. 41, 2013GL058942. doi:10.1002/2013GL058942

Boudouridis, A., 2003. Effect of solar wind pressure pulses on the size and strength of the auroral oval. J. Geophys. Res. 108. doi:10.1029/2002JA009373

Chua, D., Parks, G., Brittnacher, M., Peria, W., Germany, G., Spann, J., Carlson, C., 2001. Energy characteristics of auroral electron precipitation: A comparison of substorms and pressure pulse related auroral activity. J. Geophys. Res. Space Phys. 106, 5945–5956. doi:10.1029/2000JA003027

de la Beaujardière, O., Lyons, L.R., Ruohoniemi, J.M., Friis-Christensen, E., Danielsen, C., Rich, F.J., Newell, P.T., 1994. Quiet-Time Intensifications Along the Poleward Auroral Boundary Near Midnight. J. Geophys. Res. 99, 287–298. doi:10.1029/93JA01947

Durgonics, T., Komjathy, A., Verkhoglyadova, O., Shume, E.B., Benzon, H.-H., Mannucci, A.J., Butala, M.D., Høeg, P., Langley, R.B., 2017. Multiinstrument observations of a geomagnetic storm and its effects on the Arctic ionosphere: A case study of the 19 February 2014 storm. Radio Sci. 52, 2016RS006106. doi:10.1002/2016RS006106

Gjerloev, J.W., 2012. The SuperMAG data processing technique. J. Geophys. Res. Space Phys. 117, A09213. doi:10.1029/2012JA017683

Gkioulidou, M., Ukhorskiy, A., Mitchell, D.G., Sotirelis, T., Mauk, B., Lanzerotti, L.J., 2014. The role of small-scale ion injections in the buildup of Earth's ring current pressure: Van Allen Probes observations of the March 17th, 2013 storm. J. Geophys. Res. Space Phys. 2014JA020096. doi:10.1002/2014JA020096

Hudson, M.K., Paral, J., Kress, B.T., Wiltberger, M., Baker, D.N., Foster, J.C., Turner, D.L., Wygant, J.R., 2015. Modeling CME-shock-driven storms in 2012–2013: MHD test particle simulations. J. Geophys. Res. Space Phys. 120, 2014JA020833. doi:10.1002/2014JA020833

Juusola, L., Østgaard, N., Tanskanen, E., Partamies, N., Snekvik, K., 2011. Earthward plasma sheet flows during substorm phases. J. Geophys. Res. Space Phys. 116, A10228. doi:10.1029/2011JA016852

Kokubun, S., McPherron, R.L., Russell, C.T., 1977. Triggering of substorms by solar wind discontinuities. J. Geophys. Res. 82, 74–86. doi:10.1029/JA082i001p00074

Koustov, A.V., St.-Maurice, J.-P., Sofko, G.J., Andre, D., MacDougall, J.W., Hairston, M.R., Fiori, R.A., Kadochnikov, E.E., 2009. Three-way validation of the Rankin Inlet PolarDARN radar velocity measurements. Radio Sci. 44. doi:10.1029/2008RS004045

Lee, D.-Y., Lyons, L.R., 2004. Geosynchronous magnetic field response to solar wind dynamic pressure pulse. J. Geophys. Res. Space Phys. 109, A04201. doi:10.1029/2003JA010076

Lee, D.-Y., Lyons, L.R., Reeves, G.D., 2005. Comparison of geosynchronous energetic particle flux responses to solar wind dynamic pressure enhancements and substorms. J. Geophys. Res. Space Phys. 110, A09213. doi:10.1029/2005JA011091

Li, W., Thorne, R.M., Ma, Q., Ni, B., Bortnik, J., Baker, D.N., Spence, H.E., Reeves, G.D., Kanekal, S.G., Green, J.C., Kletzing, C.A., Kurth, W.S., Hospodarsky, G.B., Blake, J.B., Fennell, J.F., Claudepierre, S.G., 2014. Radiation belt electron acceleration by chorus waves during the 17 March 2013 storm. J. Geophys. Res. Space Phys. 119, 2014JA019945. doi:10.1002/2014JA019945

Li, Z., Hudson, M., Kress, B., Paral, J., 2015. Three-dimensional test particle simulation of the 17–18 March 2013 CME shock-driven storm. Geophys. Res. Lett. 42, 2015GL064627. doi:10.1002/2015GL064627

Liou, K., Newell, P.T., Meng, C.-I., Wu, C.-C., Lepping, R.P., 2003. Investigation of external triggering of substorms with Polar ultraviolet imager observations. J. Geophys. Res. Space Phys. 108, 1364. doi:10.1029/2003JA009984

Loto'aniu, T.M., Singer, H.J., Rodriguez, J.V., Green, J., Denig, W., Biesecker, D., Angelopoulos, V., 2015. Space weather conditions during the Galaxy 15 spacecraft anomaly. Space Weather 13, 2015SW001239. doi:10.1002/2015SW001239

Lyons, L.R., 2005. Global auroral responses to abrupt solar wind changes: Dynamic pressure, substorm, and null events. J. Geophys. Res. 110. doi:10.1029/2005JA011089

Lyons, L.R., Gallardo-Lacourt, B., Zou, S., Weygand, J.M., Nishimura, Y., Li, W., Gkioulidou, M., Angelopoulos, V., Donovan, E.F., Ruohoniemi, J.M., Anderson, B.J., Shepherd, S.G., Nishitani, N., 2016. The 17 March 2013 storm: Synergy of observations related to electric field modes and their ionospheric and magnetospheric Effects. J. Geophys. Res. Space Phys. 121, 2016JA023237. doi:10.1002/2016JA023237

Lyons, L.R., Nishimura, Y., Kim, H.-J., Donovan, E., Angelopoulos, V., Sofko, G., Nicolls, M., Heinselman, C., Ruohoniemi, J.M., Nishitani, N., 2011. Possible connection of polar cap flows to pre- and post-substorm onset PBIs and streamers. J. Geophys. Res. 116, 14 PP. doi:201110.1029/2011JA016850

Lyons, L.R., Zesta, E., Samson, J.C., Reeves, G.D., 2000. Auroral disturbances during the January 10, 1997 magnetic storm. Geophys. Res. Lett. 27, PP. 3237-3240. doi:200010.1029/1999GL000014

McPherron, R.L., 1970. Growth phase of magnetospheric substorms. J. Geophys. Res. 75, 5592–5599. doi:10.1029/JA075i028p05592

Mende, S.B., Harris, S.E., Frey, H.U., Angelopoulos, V., Russell, C.T., Donovan, E., Jackel, B., Greffen, M., Peticolas, L.M., 2008. The THEMIS Array of Ground-based Observatories for the Study of Auroral Substorms. Space Sci. Rev. 141, 357–387. doi:10.1007/s11214-008-9380-x

Nishimura, Y., Lyons, L.R., Zou, S., Xing, X., Angelopoulos, V., Mende, S.B., Bonnell, J.W., Larson, D., Auster, U., Hori, T., Nishitani, N., Hosokawa, K., Sofko, G., Nicolls, M., Heinselman, C., 2010. Preonset time sequence of auroral substorms: Coordinated observations by all-sky imagers, satellites, and radars. J. Geophys. Res. 115. doi:10.1029/2010JA015832

Ohtani, S., Yoshikawa, A., 2016. The initiation of the poleward boundary intensification of auroral emission by fast polar cap flows: A new interpretation based on ionospheric polarization. J. Geophys. Res. Space Phys. 121, 2016JA023143. doi:10.1002/2016JA023143

Paxton, L., Meng, C., Fountain, G., Ogorzalek, B., Darlington, E., Gary, S., Goldsten, J., Kusnierkiewicz, D., Lee, S., Linstrom, L., Maynard, J., Peacock, K., Persons, D., Smith, B., 1992. Special Sensor Ultraviolet Spectrographic Imager (ssusi) - an Instrument Description. Spie - Int Soc Optical Engineering, Bellingham.

Paxton, L.J., Christensen, A.B., Humm, D.C., Ogorzalek, B.S., Pardoe, C.T., Morrison, D., Weiss, M.B., Crain, W., Lew, P.H., Mabry, D.J., Goldsten, J.O., Gary, S.A., Persons, D.F., Harold, M.J., Alvarez, E.B., Ercol, C.J., Strickland, D.J., Meng, C.-I., 1999. Global ultraviolet imager (GUVI): measuring composition and energy inputs for the NASA Thermosphere Ionosphere Mesosphere Energetics and Dynamics (TIMED) mission. pp. 265–276. doi:10.1117/12.366380

Paxton, L.J., Schaefer, R.K., Zhang, Y., Kil, H., 2017. Far ultraviolet instrument technology. J. Geophys. Res. Space Phys. 122, 2016JA023578. doi:10.1002/2016JA023578

Paxton, L.J., Spisz, T., Crowley, G., Gary, R., Hopkins, M.M., Morrison, D., Wiess, M., Fountain, G.H., Suther, L., Meng, C.-I., Strickland, D.J., 1998. Interactive interpretation and display of far Ultraviolet Data. Adv. Space Res. 22, 1577–1582. doi:10.1016/S0273-1177(99)00116-7

Pitkänen, T., Aikio, A.T., Juusola, L., 2013. Observations of polar cap flow channel and plasma sheet flow bursts during substorm expansion. J. Geophys. Res. Space Phys. 118, 774–784. doi:10.1002/jgra.50119

Shi, Y., Zesta, E., Lyons, L.R., Yang, J., Boudouridis, A., Ge, Y.S., Ruohoniemi, J.M., Mende, S., 2012. Two-dimensional ionospheric flow pattern associated with auroral streamers. J. Geophys. Res. 117. doi:10.1029/2011JA017110

Waters, C.L., Anderson, B.J., Liou, K., 2001. Estimation of global field aligned currents using the iridium® System magnetometer data. Geophys. Res. Lett. 28, 2165–2168. doi:10.1029/2000GL012725

Yue, C., Nishimura, Y., Lyons, L.R., Angelopoulos, V., Donovan, E.F., Shi, Q., Yao, Z., Bonnell, J.W., 2013. Coordinated THEMIS spacecraft and all-sky imager observations of interplanetary shock effects on plasma sheet flow bursts, poleward boundary intensifications, and streamers. J. Geophys. Res. Space Phys. 118, 3346–3356. doi:10.1002/jgra.50372

Zesta, E., Singer, H.J., Lummerzheim, D., Russell, C.T., Lyons, L.R., Brittnacher, M.J., 2000. The Effect of the January 10, 1997, Pressure Pulse on the Magnetosphere-Ionosphere Current System, in: Ohtani, S.-I., Fujii, R., Hesse, M., Lysak, R.L. (Eds.), Magnetospheric Current Systems. American Geophysical Union, pp. 217–226.

Zhou, X., Tsurutani, B.T., 2001. Interplanetary shock triggering of nightside geomagnetic activity: Substorms, pseudobreakups, and quiescent events. J. Geophys. Res. Space Phys. 106, 18957–18967. doi:10.1029/2000JA003028

Zou, Y., Nishimura, Y., Lyons, L.R., Donovan, E.F., Ruohoniemi, J.M., Nishitani, N., McWilliams, K.A., 2014. Statistical relationships between enhanced polar cap flows and PBIs. J. Geophys. Res. Space Phys. 119, 2013JA019269. doi:10.1002/2013JA019269

Zou, Y., Nishimura, Y., Lyons, L.R., Donovan, E.F., Shiokawa, K., Ruohoniemi, J.M., McWilliams, K.A., Nishitani, N., 2015. Polar Cap Precursor of Nightside Auroral Oval Intensifications Using Polar Cap Arcs. J. Geophys. Res. Space Phys. 2015JA021816. doi:10.1002/2015JA021816

Figure 1: From top to bottom, the WIND P_{dyn}, the OMNI IMF, the SuperMAG upper U and lower L magnetic index, and the SuperMAG ring current index for all MLT and within the dusk, noon, dawn, and midnight sectors on 17 March 2013. At the bottom are magnetic perturbations observed along Iridium satellite trajectories during the two 10 min intervals identified by the purple arrows. Red and blue shadings give upward and downward radial current, respectively, obtained from the curl of fits to the magnetic perturbations (based on Figurers 1 and 6 of Paper 1).

Figure 2: Representative mergers of auroral images over Canada from the array of THEMIS ASIs for the shock impact event on 17 March 2013 overlaid with LOS flow velocities from the SuperDARN radars. UT times are given in the upper left comer of each panel. LOS flow velocities within the polar cap are primarily from Inuvik to the west and Rankin Inlet to the east. There are also some LOS velocities from the from lower latitude SuperDARN radars. Yellow ellipses encircle the enhanced anti-sunward LOS flows seen within the polar cap by the radars after the shock impact.

Figure 3: Auroral images over the southern hemisphere from the Special Sensor Ultraviolet Spectrographic Imager onboard polar-orbiting DMSP spacecraft at the LBH2 (165-180 nm) (135.6 nm/) band. The images are essentially keograms made along space trajectories from horizon to horizon imager scans in the direction normal to the trajectory. Precipitating electron energy fluxes measured along the DMSP trajectories are color coded along the trajectories. Flows measures by the DMSP F17 and F16 spacecraft in the direction normal to the spacecraft trajectory are shown by violet bars normal along the trajectories. UT times indicated along each trajectory.

Figure 4: (modify to make SuperDARN flows scales the same) Precipitating electron energy fluxes from both the POES (left panel) and DMSP (right panel) spacecraft

over the southern hemisphere. Polar cap flows seen by the southern hemisphere SuperDARN radars at times during the period of rapid auroral poleward expansion are also shown, as are the flows measures by the DMSP F17 and F16 spacecraft in the direction normal to the spacecraft trajectory (black bars along the trajectories). UT times indicated along each trajectory

Figure 5: From top to bottom, the OMNI P_{dyn}, the OMNI IMF, the SuperMAG upper U and lower L magnetic index, and the SuperMAG ring current index for all MLT and within the dusk, noon, dawn, and midnight sectors on 19 March 2014.

Figure 6: Same as Figure 2, except for19 February 2014.

Figure 7: SuperDARN LOS flows in the southern hemisphere for times before and after the shock impact on 19 February 2014. Precipitating electron energy fluxes from the POES spacecraft that are shown in the fourth panel, with UT times indicated along each trajectory.

Figure 8: SuperDARN LOS flows in the northern hemisphere for times before after the shock impact on 5 April 2015.

Figure 9: Mergers of images from the THEMIS ASIs overlaid with LOS flow velocities from the SuperDARN radars for selected times during an event that started as a typical substorm onset at ~0803 UT on 13 October 2010.

Supplemental Movie: Mergers of images from the THEMIS ASIs overlaid with LOS flow velocities from the SuperDARN radars at the high possible time resolution (3 s) of the ASIs during the event that started as a typical substorm onset at ~0803 UT on 13 October 2010. Time resolution of the radar observations is 2 min.

.

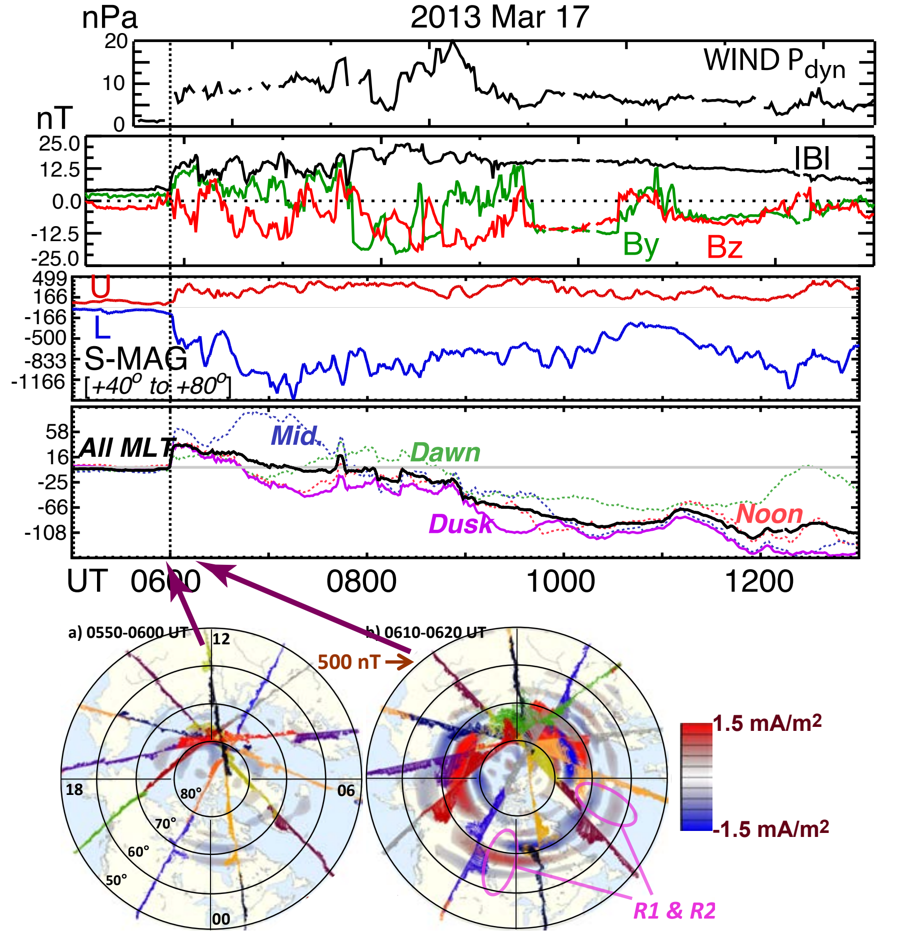

2013 Mar 17
nPa
WIND Pdyn
20
10
0
nT
IBI
25.0
12.5
0.0
-12.5
-25.0
By
Bz
U
L
499
166
-166
-500
-833
-1166
S-MAG
[+40° to +80°]
All MLT
Mid.
Dawn
Dusk
Noon
58
16
-25
-66
-108
UT
0600
0800
1000
1200
a) 0550-0600 UT
b) 0610-0620 UT
500 nT
12
18
06
00
80°
70°
60°
50°
1.5 mA/m2
-1.5 mA/m2
R1 & R2

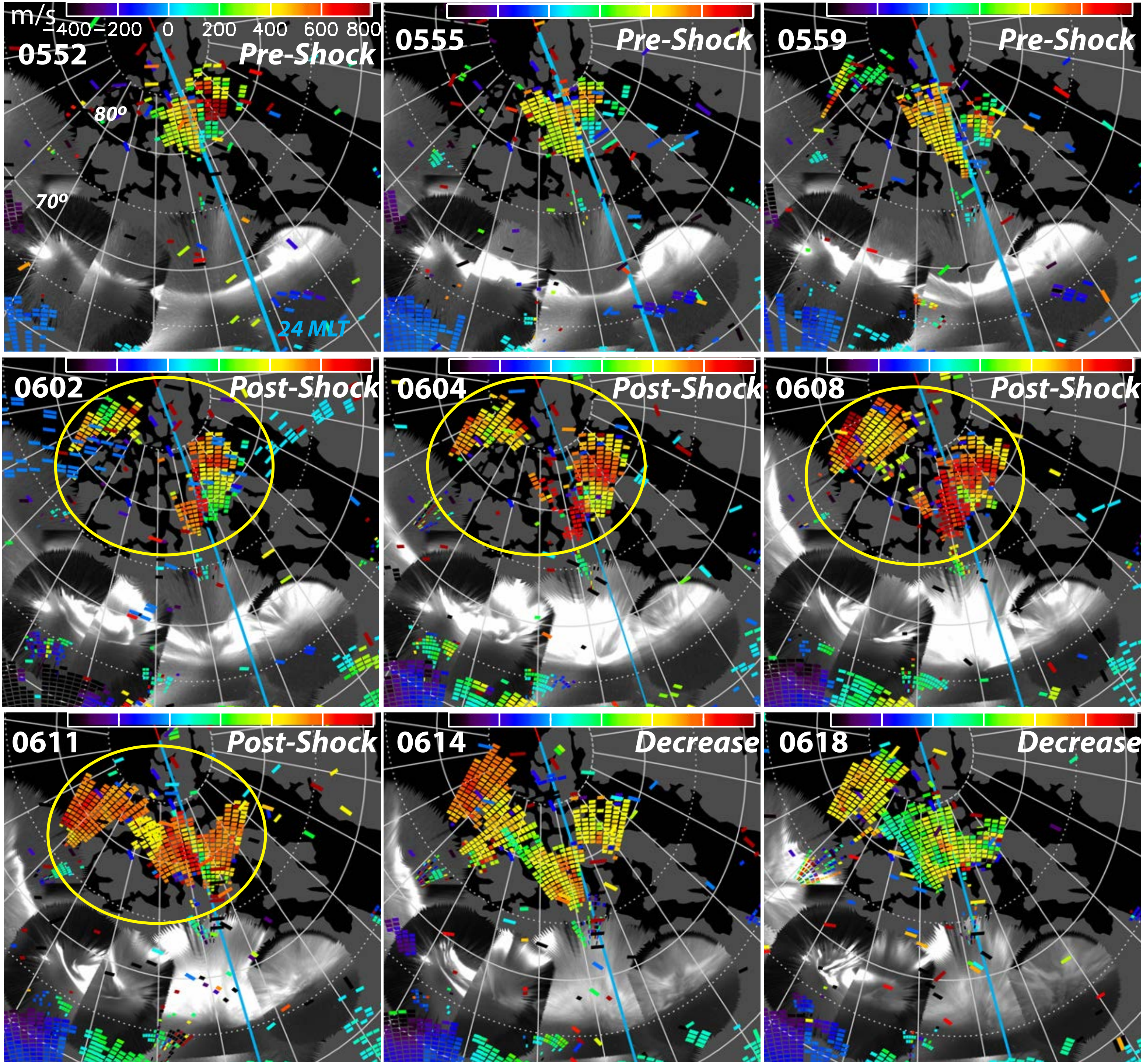
m/s
−400 −200 0 200 400 600 800
0552
Pre-Shock
80°
70°
24 MLT
0555
Pre-Shock
0559
Pre-Shock
0602
Post-Shock
0604
Post-Shock
0608
Post-Shock
0611
Post-Shock
0614
Decrease
0618
Decrease

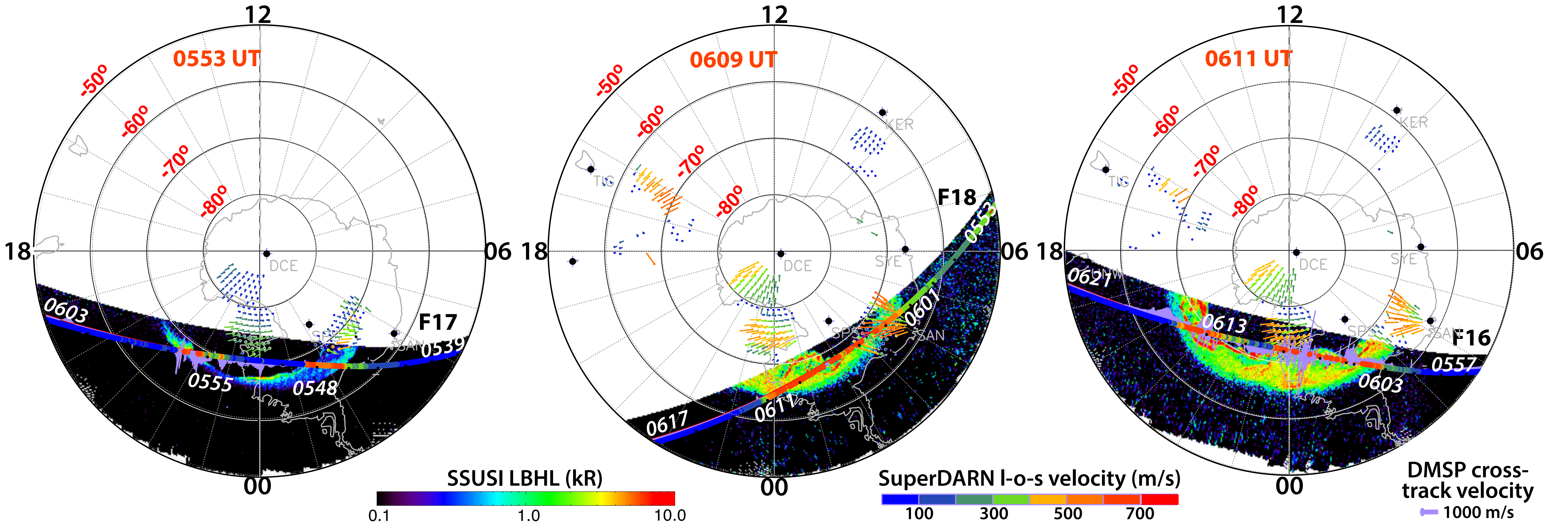

0553 UT
0609 UT
0611 UT
12
18
06
00
-50°
-60°
-70°
-80°
DCE
KER
SYE
SAN
TIG
F17
F18
F16
0603
0555
0548
0539
0617
0611
0601
0553
0621
0613
0603
0557
SSUSI LBHL (kR)
0.1
1.0
10.0
SuperDARN l-o-s velocity (m/s)
100
300
500
700
DMSP cross-track velocity
1000 m/s

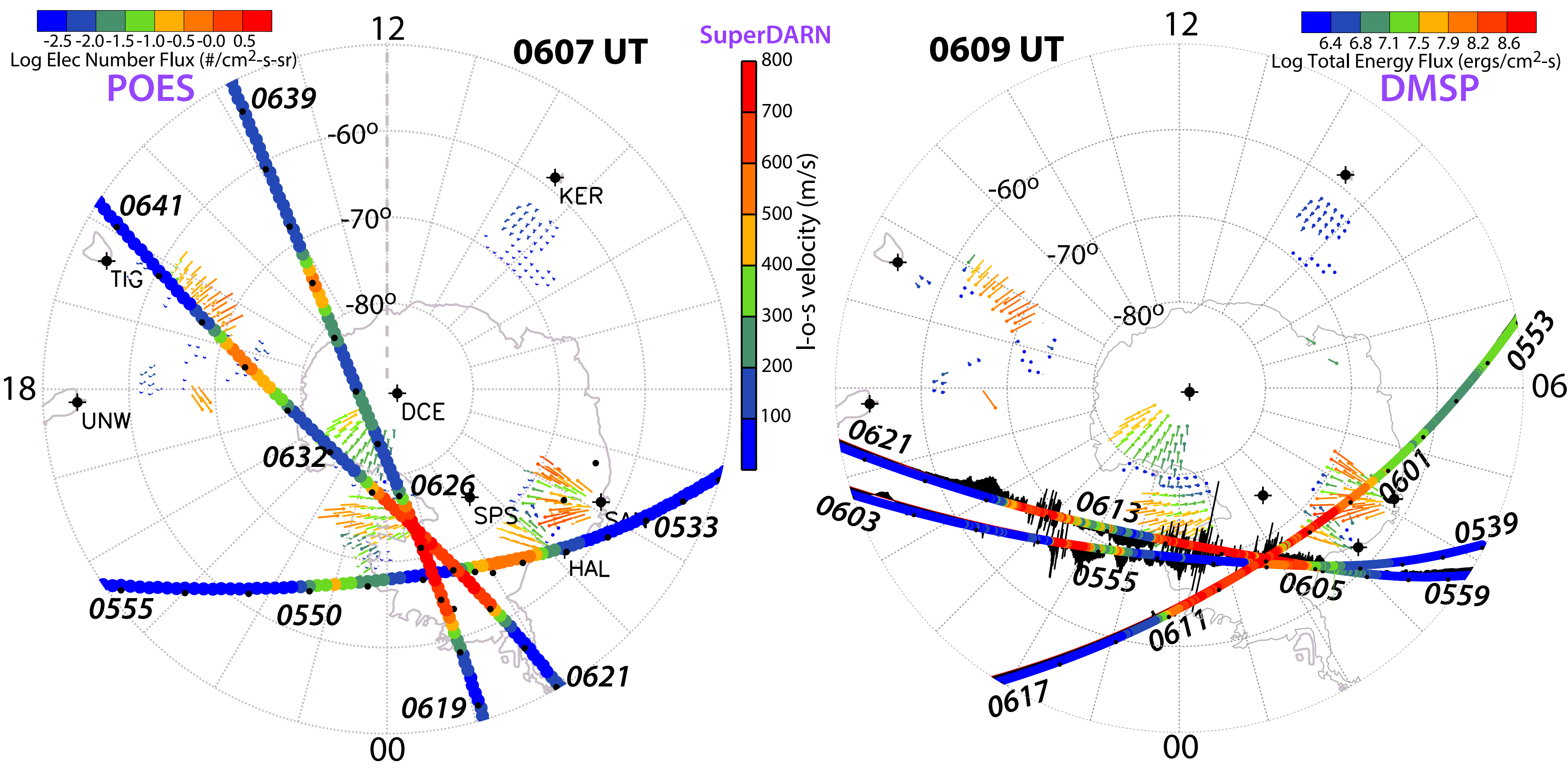

-2.5 -2.0 -1.5 -1.0 -0.5 -0.0 0.5
Log Elec Number Flux (#/cm2-s-sr)
POES
12
0607 UT
SuperDARN
800
700
600
500
400
300
200
100
l-o-s velocity (m/s)
0639
-60o
-70o
-80o
KER
0641
TIG
18
UNW
DCE
0632
0626
SPS
0533
HAL
0555
0550
0621
0619
00
0609 UT
12
6.4 6.8 7.1 7.5 7.9 8.2 8.6
Log Total Energy Flux (ergs/cm2-s)
DMSP
-60o
-70o
-80o
0553
06
0621
0601
0613
0603
0539
0555
0605
0559
0611
0617
00

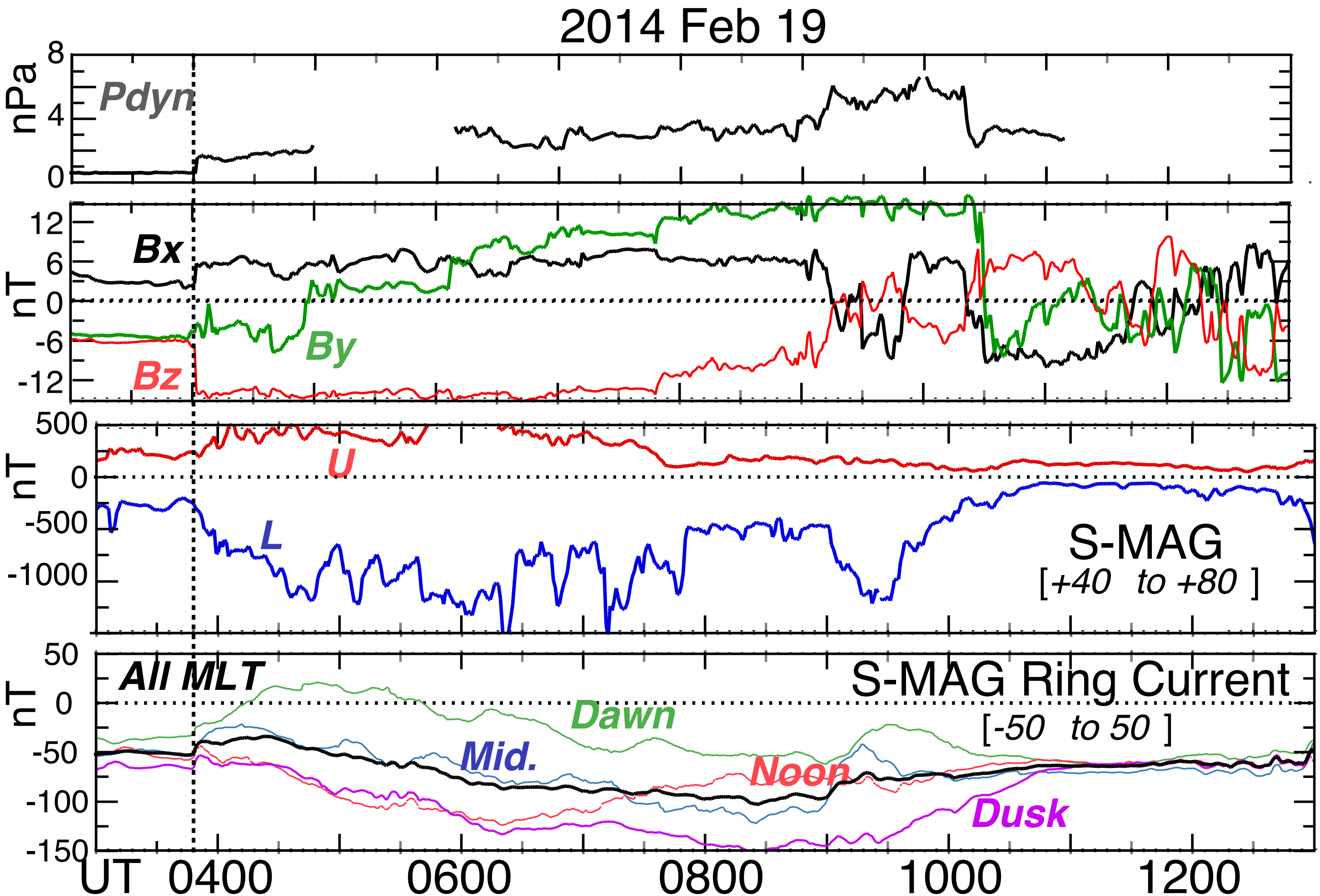

2014 Feb 19
nPa
8
4
0
Pdyn
nT
12
6
0
-6
-12
Bx
By
Bz
nT
500
0
-500
-1000
U
L
S-MAG
[+40 to +80]
nT
50
0
-50
-100
-150
All MLT
S-MAG Ring Current
[-50 to 50]
Dawn
Mid.
Noon
Dusk
UT 0400
0600
0800
1000
1200

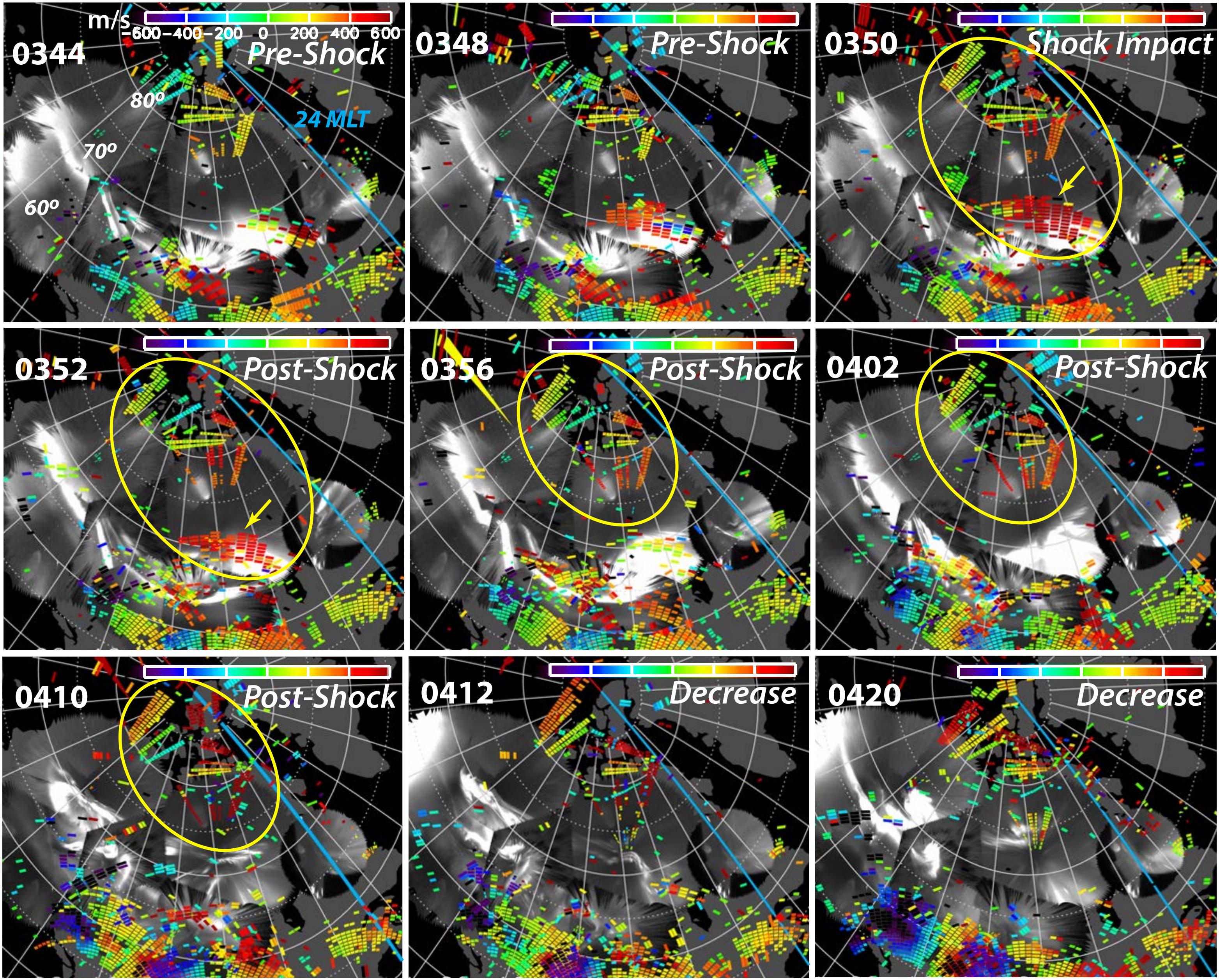

m/s
-600 -400 -200 0 200 400 600
0344
Pre-Shock
80º
70º
60º
24 MLT
0348
Pre-Shock
0350
Shock Impact
0352
Post-Shock
0356
Post-Shock
0402
Post-Shock
0410
Post-Shock
0412
Decrease
0420
Decrease

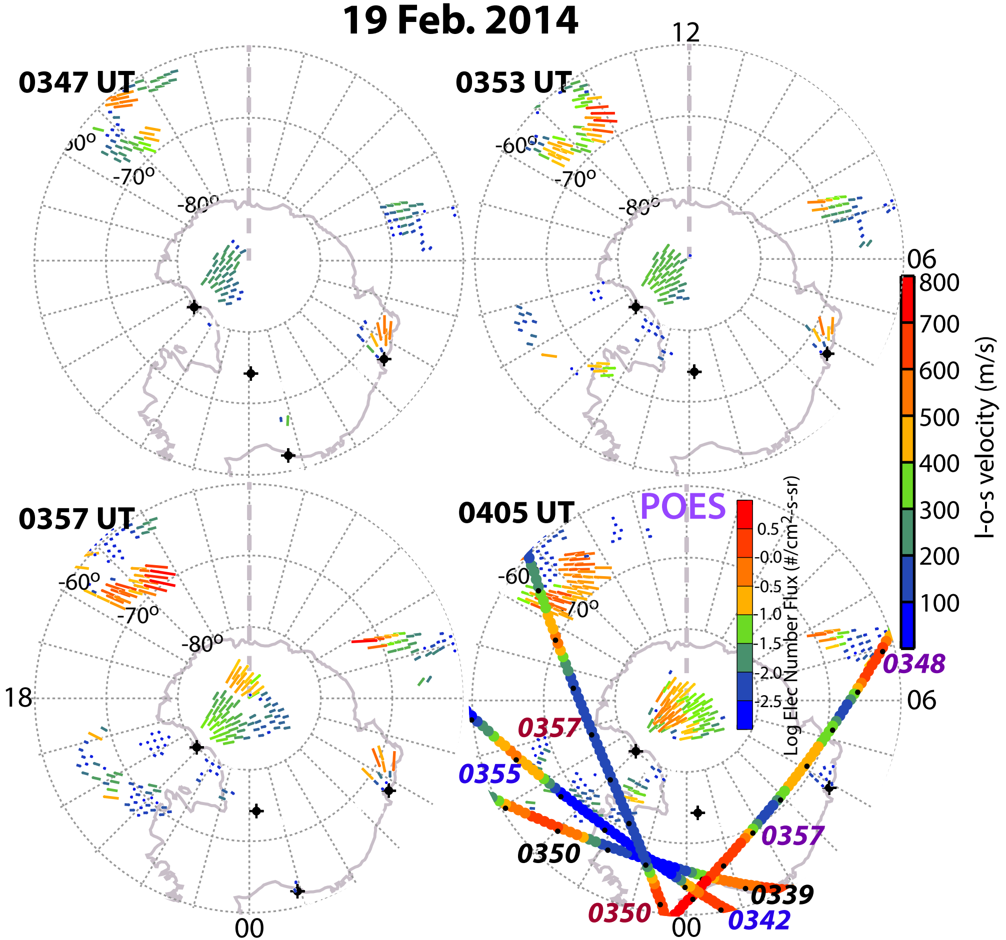
19 Feb. 2014
0347 UT
0353 UT
0357 UT
0405 UT
POES
12
06
18
00
-60o
-70o
-80o
l-o-s velocity (m/s)
800
700
600
500
400
300
200
100
Log Elec Number Flux (#/cm2-s-sr)
0.5
-0.0
-0.5
-1.0
-1.5
-2.0
-2.5
0348
0357
0355
0350
0339
0342

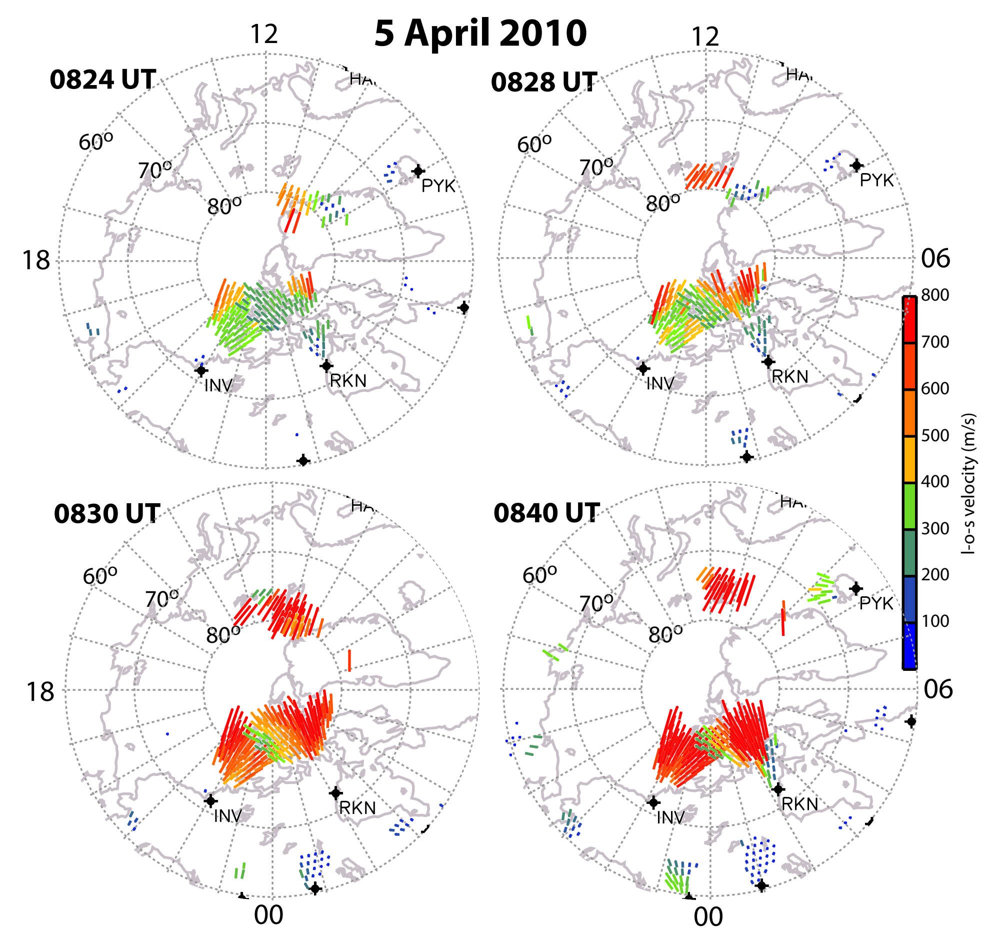

5 April 2010
0824 UT
0828 UT
0830 UT
0840 UT
12
18
06
00
60°
70°
80°
PYK
INV
RKN
800
700
600
500
400
300
200
100
l-o-s velocity (m/s)

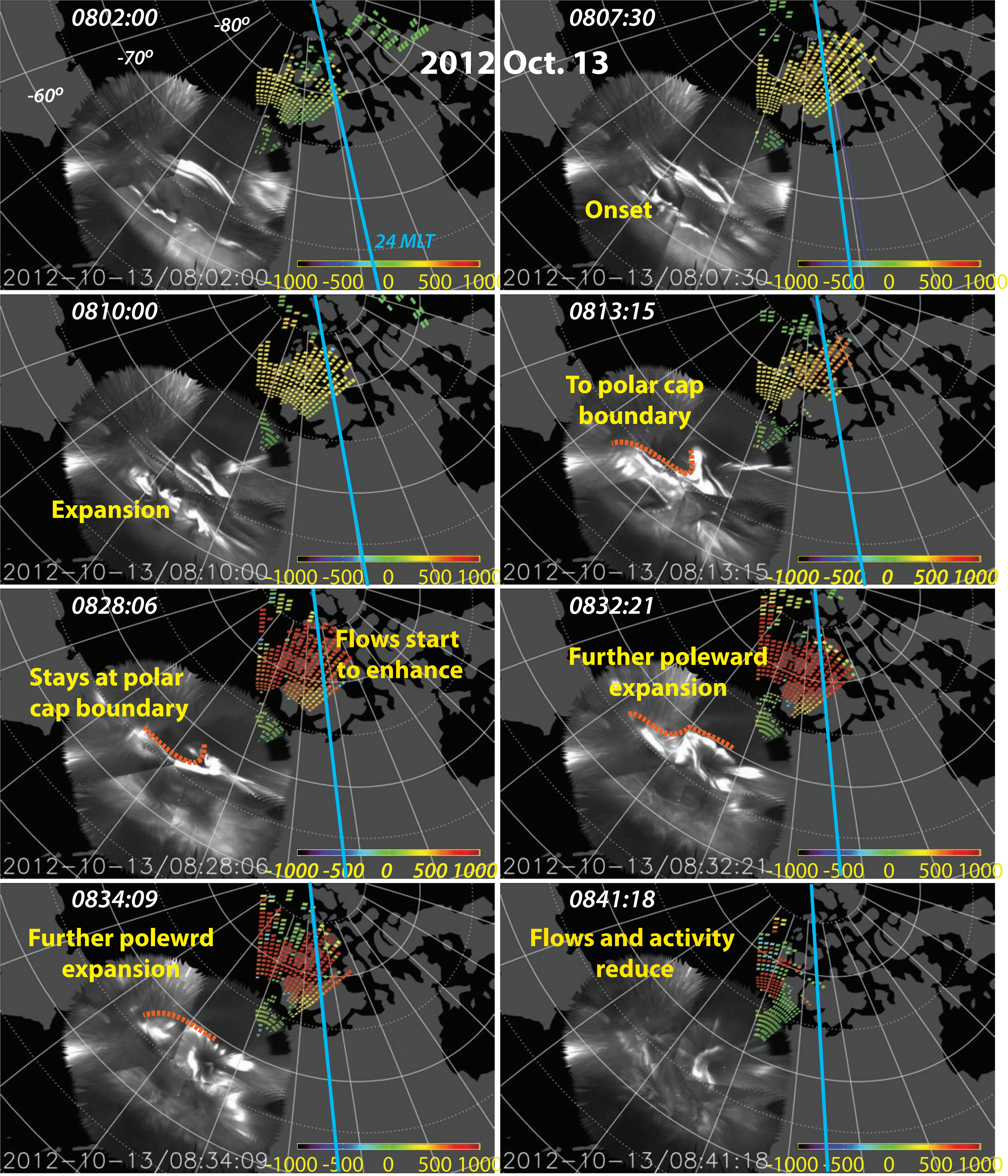
2012 Oct. 13
0802:00
-80°
-70°
-60°
24 MLT
2012-10-13/08:02:00
-1000 -500 0 500 1000
0807:30
Onset
2012-10-13/08:07:30
-1000 -500 0 500 1000
0810:00
Expansion
2012-10-13/08:10:00
-1000 -500 0 500 1000
0813:15
To polar cap boundary
2012-10-13/08:13:15
-1000 -500 0 500 1000
0828:06
Stays at polar cap boundary
Flows start to enhance
2012-10-13/08:28:06
-1000 -500 0 500 1000
0832:21
Further poleward expansion
2012-10-13/08:32:21
-1000 -500 0 500 1000
0834:09
Further polewrd expansion
2012-10-13/08:34:09
-1000 -500 0 500 1000
0841:18
Flows and activity reduce
2012-10-13/08:41:18
-1000 -500 0 500 1000